SCIENTIFIC REPORTS
nature research

OPEN

Therapeutic targeting of 15-PGDH in murine pulmonary fibrosis

Julianne N. P. Smith[1], Matthew D. Witkin[1], Alvin P. Jogasuria[1], Kelsey F. Christo[1], Thomas M. Raffay[1], Sanford D. Markowitz[1,2]✉ & Amar B. Desai[1]✉

Idiopathic pulmonary fibrosis (IPF) is a progressive disease characterized by interstitial remodeling and pulmonary dysfunction. The etiology of IPF is not completely understood but involves pathologic inflammation and subsequent failure to resolve fibrosis in response to epithelial injury. Treatments for IPF are limited to anti-inflammatory and immunomodulatory agents, which are only partially effective. Prostaglandin E2 (PGE2) disrupts TGFβ signaling and suppresses myofibroblast differentiation, however practical strategies to raise tissue PGE2 during IPF have been limited. We previously described the discovery of a small molecule, (+)SW033291, that binds with high affinity to the PGE2-degrading enzyme 15-hydroxyprostaglandin dehydrogenase (15-PGDH) and increases PGE2 levels. Here we evaluated pulmonary 15-PGDH expression and activity and tested whether pharmacologic 15-PGDH inhibition (PGDHi) is protective in a mouse model of bleomycin-induced pulmonary fibrosis (PF). Long-term PGDHi was well-tolerated, reduced the severity of pulmonary fibrotic lesions and extracellular matrix remodeling, and improved pulmonary function in bleomycin-treated mice. Moreover, PGDHi attenuated both acute inflammation and weight loss, and decreased mortality. Endothelial cells and macrophages are likely targets as these cell types highly expressed 15-PGDH. In conclusion, PGDHi ameliorates inflammatory pathology and fibrosis in murine PF, and may have clinical utility to treat human disease.

Idiopathic pulmonary fibrosis (IPF) is a progressive and irreversible disease involving the accumulation of extracellular matrix (ECM) throughout alveoli and interstitial spaces, leading to the destruction of lung parenchyma and impaired gas exchange[1]. Although the precise etiology of IPF is unknown, the median age of onset is 66[2], likely due to dysfunctional wound healing[3], heightened inflammation, and a reduced ability to resolve fibrosis[4] as an organism ages. Anti-fibrotic agents are commonly used to treat IPF and extend the 3–4 year estimated survival seen in untreated IPF patients[2]. However, novel therapeutic approaches to further limit IPF pathogenesis and mitigate IPF severity are needed.

The initiation of IPF is often characterized by early recurrent lung epithelial injuries that are not cleared and eventually lead to the deposition of fibrosis. Although anti-inflammatory therapies to date have provided little benefit in IPF trials[5], studies suggest that immune responses are involved in disease development and progression[6]. Indeed, neutrophils accumulate in IPF patient lungs[7–9], and neutralizing neutrophil-derived products mitigates murine IPF severity[10,11]. Monocyte-derived alveolar macrophages are also implicated in human IPF[12]. Notably, classically-activated, or M1, macrophages produce potent pro-inflammatory cytokines including TNFα, IL-1, and IL-6[13]. In response to chronic inflammation, M1 macrophages take on characteristics of alternatively-activated, or M2, macrophages[14], which contribute to fibrosis and collagen synthesis via production of transforming growth factor-β (TGFβ), platelet-derived growth factor (PDGF), and upregulation of L-arginine metabolism[13].

Fibroblasts play a key role in IPF pathology through their proliferation, migration, and differentiation to myofibroblasts. TGFβ drives the differentiation of fibroblasts to myofibroblasts via the induction of various cellular processes and signaling cascades, including Smad protein activation, phosphatidylinositol 3-kinase/Akt, ERK and MAPK signaling, and cytosolic calcium oscillation[15,16]. Engagement of these signaling pathways results in the expression of ECM proteins, and the formation of stress fibers. Several lung-resident and circulating cell types produce PGE2 upon inflammation, and specifically following bleomycin-induced lung injury, including pulmonary fibroblasts, alveolar epithelial cells, and monocyte/macrophage lineage cells[17,18]. Signaling via PGE2

[1]Department of Medicine, and Case Comprehensive Cancer Center, Case Western Reserve University, Cleveland, OH 44106, USA. [2]University Hospitals Seidman Cancer Center, Cleveland, OH 44106, USA. ✉email: sxm10@case.edu; Abd10@case.edu

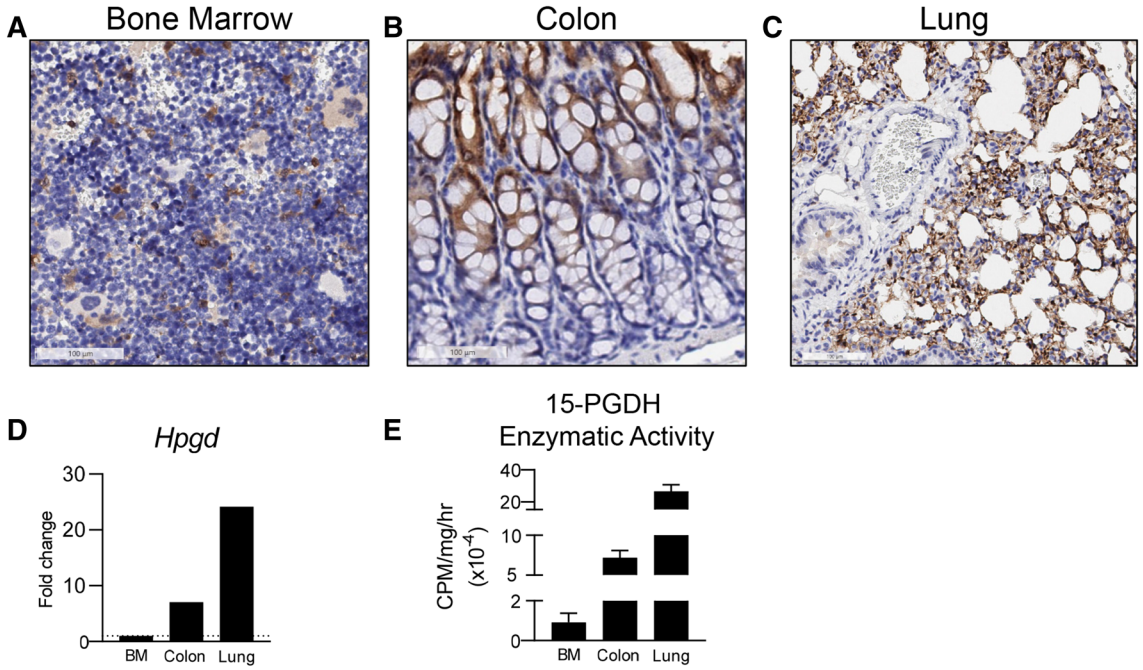

Figure 1. 15-PGDH is highly expressed in the murine lung. (**A**–**C**) Representative images of 15-PGDH staining (brown) in healthy murine bone marrow (BM), colon, and lung, with Hematoxylin counter stain. 20X, scale bars represent 100 μm, as indicated. (**D**) Relative gene expression of *Hpgd* in murine BM, colon, and lung by RT-PCR, normalized to *B2m* levels and expressed as fold change relative to the level in BM. (**E**) 15-PGDH enzymatic activity in murine BM, colon, and lung, as measured in counts per minute (CPM) over one hour and normalized to input protein (in mg).

receptors EP2 and EP4 antagonizes TGFβ-induced pro-fibrotic signaling, suggesting that this axis is critical for normal pulmonary tissue repair and regeneration. Endogenous PGE2 production is likely insufficient to block pathogenesis due to the reduced expression of EP2 and EP4 in fibrotic lung tissue[19,20], however. Therefore, well-tolerated strategies to increase pulmonary PGE2 levels are likely to mitigate pathogenesis. Indeed, recent reports have demonstrated that either systemic administration of the long-acting PGE2 analog 16,16-dimethyl-PGE2[18], or targeted PGE2 delivery via pulmonary endothelial cell-specific antibodies or inhalation of PGE2-loaded liposomes[21,22] demonstrate therapeutic efficacy in murine pulmonary fibrosis. In vitro, PGE2 stimulation or EP2/EP4-specific agonism abrogates myofibroblast differentiation and expression of ECM genes in TGFβ-treated human pulmonary fibroblasts and in fibroblasts derived from IPF patients[19,23–25]. Thus, we hypothesized that increasing endogenous PGE2 by systemic administration of well-tolerated small molecules that inhibit the PGE2-degrading enzyme 15-hydroxyprostaglandin dehydrogenase (15-PGDH) would prevent pulmonary fibrosis in bleomycin-treated mice.

Results

15-PGDH is highly expressed and active in healthy murine lung tissue. (+)SW033291 is known to increase systemic PGE2 levels and enhance tissue regeneration[26]. To determine if 15-PGDH may be targetable in the murine lung, we first examined its expression in the lungs of healthy mice, relative to other organs in which 15-PGDH inhibitors (PGDHi) have demonstrated therapeutic efficacy[26,27]. Immunohistochemical staining revealed subsets of PGDH+ hematopoietic cells in the bone marrow (BM) and numerous PGDH+ cells in the colonic epithelium (Fig. 1A,B). In contrast, 15-PGDH was highly expressed throughout the lung parenchyma (Fig. 1C), suggesting pulmonary tissue may also be responsive to PGDH inhibition. We further compared expression of *Hpgd*, the gene that encodes 15-PGDH, in colonic and pulmonary tissue relative to BM. Lung tissue homogenates displayed 25- and 3-fold higher *Hpgd* gene expression than BM and colon, respectively (Fig. 1D). To confirm that pulmonary 15-PGDH is functional and therefore capable of regulating local PGE2 levels, we next measured specific enzymatic activity in homogenates from the same organs. Lung tissue demonstrated >200- and 3.7-fold higher activity per milligram total protein than BM and colonic tissue, respectively (Fig. 1E). Together these data demonstrate that 15-PGDH is abundantly expressed and highly enzymatically active in the murine lung and provide rationale for pharmacologic targeting of 15-PGDH as a strategy to increase local PGE2 and limit the pathogenesis of pulmonary fibrosis (PF).

PGDHi mitigates early bleomycin-induced inflammation. In mice, administration of bleomycin results in lung injury that mimics key aspects of human IPF[28], with an initial inflammatory phase followed by a subsequent fibrotic phase[29]. To study the effects of 15-PGDH inhibition in PF, we administered bleomycin intravenously and began twice daily treatment of mice with (+)SW033291 (PGDHi) or vehicle control (Fig. 2A).

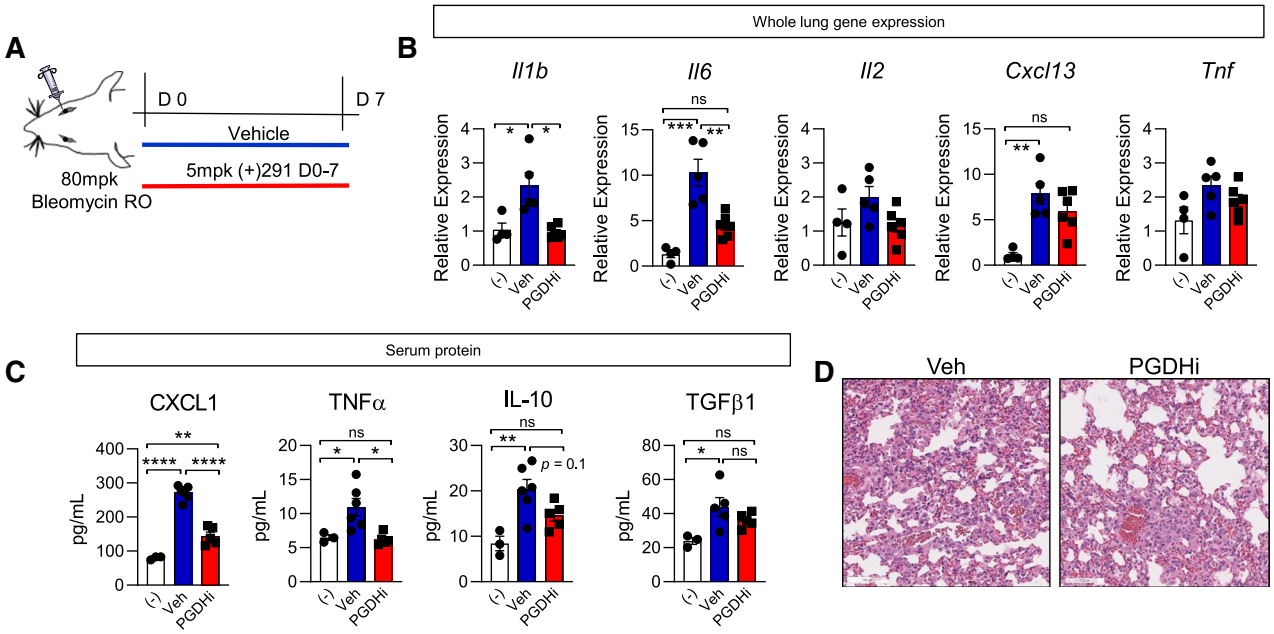

Figure 2. PGDHi mitigates bleomycin-induced inflammation. (**A**) Schematic depicting retro-orbital (RO) administration of 80 mg/kg Bleomycin to 8wk old C57BL/6 female mice with subsequent PGDHi therapy (5 mg/kg (+)SW033291, i.p. twice per day) and sacrifice at day 7. (**B**) Inflammatory factors *Il1b, Il6, Il2, Cxcl13, and Tnf* were quantified in lung homogenates isolated from naïve healthy control mice (−), and vehicle (Veh) and PGDHi-treated mice 7 days post-bleomycin administration by RT-PCR and are expressed relative to *B2m* levels. For *Il1b* and *Cxcl13*, Kruskal–Wallis test with post-hoc Dunn's multiple comparisons tests were performed; for *Il6*, *Il2*, and *Tnf*, ordinary one-way ANOVA with post-hoc Tukey multiple comparisons tests were performed. (**C**) Inflammatory and fibrogenic factors CXCL1, TNFα, IL-10, and TGFβ were measured in the serum of healthy naïve (−), and Veh- and PGDHi-treated mice 7 days post-bleomycin administration by multiplex ELISA. Individual data points and mean ± SEM are depicted; n = 5–6 experimental mice/group. Ordinary one-way ANOVA with post-hocTukey multiple comparisons tests were used to compare groups for all factors. (**D**) Representative hematoxylin and eosin-stained lung sections from vehicle- and PGDHi-treated mice 7 days post-bleomycin administration. 20X, scale bars represent 100 μm. ****$P < 0.0001$, ***$P = 0.0001$, **$P < 0.005$, *$P < 0.05$ for indicated comparisons.

PGDHi attenuated early pulmonary inflammation, as evidenced by greater than 50% reductions in *Il1b* and *Il6* expression in lung tissue 7 days post-bleomycin exposure, in addition to moderate reductions in the expression of other inflammation-associated genes (Fig. 2B). These data indicate that inhibiting 15-PGDH in the context of bleomycin-induced lung injury may limit pathologic inflammation in the lung. Moreover, PGDHi treatment was associated with significantly lower levels of the neutrophil chemoattractant CXCL1, the cytokine TNFα, and a trend towards reduced IL-10 in the serum (Fig. 2C). CXCL1 and TNFα were also reduced in PGDHi-treated mice exposed to bleomycin intratracheally (Supplementary Fig. 1A–B). TNFα promotes TGFβ1 expression[30], and although IL-10 limits inflammation in many contexts, it is thought to promote fibroblast proliferation in PF[31], therefore these changes likely have an anti-fibrotic effect on injured pulmonary tissue. Of note, TGFβ1 was elevated in the serum of vehicle-treated mice 7 days post-bleomycin exposure and PGDHi treatment led to a moderate but statistically insignificant reduction (44 ± 5.5 vs. 36 ± 1.9 pg/mL). Additionally, while vehicle-treated mice displayed alveolar wall thickening and an abundance of small alveolar spaces, a trend towards greater alveolar size was observed with PGDHi (Fig. 2D). Analysis of the lungs of mice 14 days post-intratracheal bleomycin administration demonstrated similar morphological changes (Supplementary Fig. 1C). These data therefore indicate that PGDHi limits both systemic and local inflammation during the early phase of bleomycin-induced lung injury.

PGDHi improves survival in bleomycin-induced pulmonary fibrosis. The above results demonstrate that PGDHi mitigates acute inflammatory responses to bleomycin lung injury. To test whether PGDHi additionally protects against the severity of chronic fibrotic disease, we extended our analysis and continued to administer (+)SW033291 to bleomycin-exposed mice through day 35 (Fig. 3A). While vehicle-treated mice experienced severe weight loss in the first 8 days following bleomycin administration, PGDHi limited the severity and duration of weight loss (Fig. 3B and Supplementary Fig. 2A–B). Specifically, vehicle-treated mice reached a nadir of 26.8% body weight loss on day 8 post-intravenous bleomycin treatment, versus PGDHi-treated mice, which experienced only 16.0% maximum mean body weight loss on day 6 with weight stabilization thereafter. PGDHi-treated mice also achieved weight recovery closer to baseline between 21 and 28 days post-bleomycin administration, suggesting that PGDHi attenuated the effects of bleomycin on overall health. Notably, 35% of vehicle-treated mice succumbed to death, compared to 10% of PGDHi-treated mice (Fig. 3C). These results were

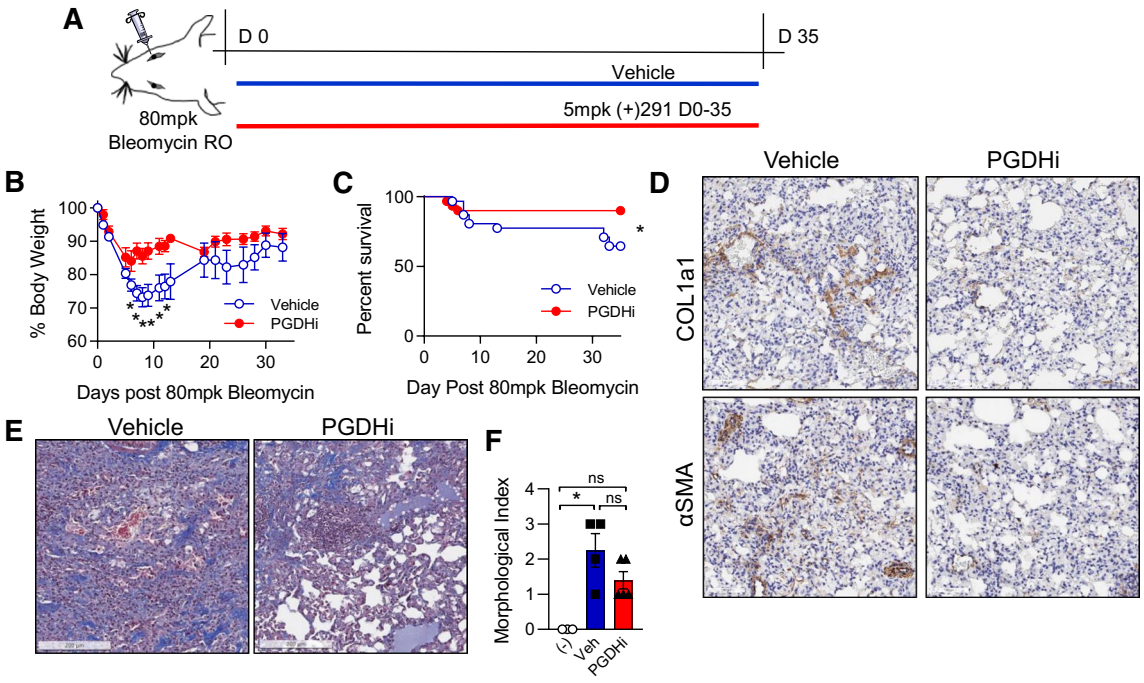

Figure 3. PGDHi improves survival in bleomycin-induced pulmonary fibrosis. (**A**) Schematic depicting retro-orbital (RO) administration of 80 mg/kg Bleomycin to 8wk old C57BL/6 female mice with subsequent PGDHi therapy (5 mg/kg (+)SW033291, twice per day) and sacrifice at day 35. (**B**) Body weight was measured for thirty-five days post-bleomycin administration as a percentage of day 0 weight for each mouse, treated as indicated. Mean ± SEM is depicted. n = 6 mice/group at the onset of the study and n = 4–5 mice/group at the end of the study. A two-way ANOVA with post-hoc Sidak's multiple comparisons test was used to compare vehicle- versus PGDHi-treated mice. (**C**) Kaplan–Meier survival curve following bleomycin administration. N = 29–30 mice per group. (**D**) Representative images depicting COL1a1 and αSMA immunohistochemical staining (brown) in day 35 lung samples from vehicle- and PGDHi-treated mice. (**E**) Representative images of Masson's trichrome-stained lung sections from vehicle- and PGDHi-treated mice 35 days post-bleomycin administration. (**F**) Pathological scoring of Masson's trichrome-stained lung sections, from healthy naïve control (−), and Veh- and PGDHi-treated mice at day 35 post-bleomycin administration, based on a semi-quantitative morphological index of lung injury. Mean ± SEM is depicted. n = 4–5 mice per group. A Kruskal–Wallis test with post-hoc Dunn's multiple comparisons test was used to compare groups. $^{*}P < 0.05$ for indicated comparisons. For micrographs, scale bars represent 100 μm.

also observed in mice exposed to bleomycin intratracheally, where 40% of vehicle- and 16% of PGDHi-treated mice succumbed to death (Supplementary Fig. 2C). Together these results suggest PGDHi therapy ameliorates systemic pathology during bleomycin-induced lung injury.

To determine the impact of PGDHi on bleomycin-induced lung fibrosis, ECM accumulation was evaluated in lung tissue 35 days post-bleomycin exposure. Importantly, pulmonary 15-PGDH expression was maintained following bleomycin administration (Supplementary Fig. 3). Lung sections from vehicle-treated mice showed regional accumulation of Collagen 1a1 (COL1a1) and alpha-smooth muscle-actin (αSMA), whereas staining was reduced and non-focal in the lungs of PGDHi-treated mice (Fig. 3D), indicating that 15-PGDH inhibition protects against severe fibrosis in bleomycin-induced PF. In addition to COL1a1, total collagen and lung morphology was evaluated on Masson's trichrome-stained lung sections. Vehicle-treated mice displayed striking collagen deposition in the lung parenchyma, thickening of alveolar septa due to increased collagen, and intra-alveolar involvement. In contrast, PGDHi-treated mice showed fewer fibrotic lesions, which were interspersed with normal architecture, and less collagen accumulation (Fig. 3E). Pathological evaluation using a semiquantitiative morphological index of lung injury[28], where 0 represents normal lung tissue and 5 represents high levels of inflammation and fibrosis throughout the surveyed lung lobes, demonstrated substantial lung injury in bleomycin-treated mice. PGDHi resulted in a trend towards lung injury reduction when compared to vehicle treatment (Fig. 3F). The anti-fibrotic impact of PGDHi was confirmed in mice 35 days post-intratracheal bleomycin treatment (Supplementary Fig. 4A), wherein PGDHi significantly decreased lung hydroxyproline levels (Supplementary Fig. 4B), and led to a trends towards preservation of lung morphology (Supplementary Fig. 4C).

PGDHi attenuates pulmonary measurements of tissue stiffness in bleomycin-treated mice. To determine whether PGDHi-mediated reductions in inflammation and histopathological features of fibrosis corresponded to functional improvements, we measured static lung compliance (Cst) by generating pressure–volume loops in anesthetized, tracheostomized mice before necropsy. PGDHi treatment attenuated the impact of bleomycin on baseline static compliance, inspiratory capacity, and cellular content of the bron-

A

Group	% Weight	Compliance	Inspiratory Capacity	BALF cells
Naïve	100	0.056 ± 0.003	0.596 ± 0.024	2.72e4 ± 2.47e3
Vehicle	85.6 ± 2.6	0.040 ± 0.003	0.479 ± 0.029	2.66e5 ± 5.55e4
PGDHi	96.8 ± 1.2	0.048 ± 0.002	0.533 ± 0.015	1.11e5 ± 2.38e4

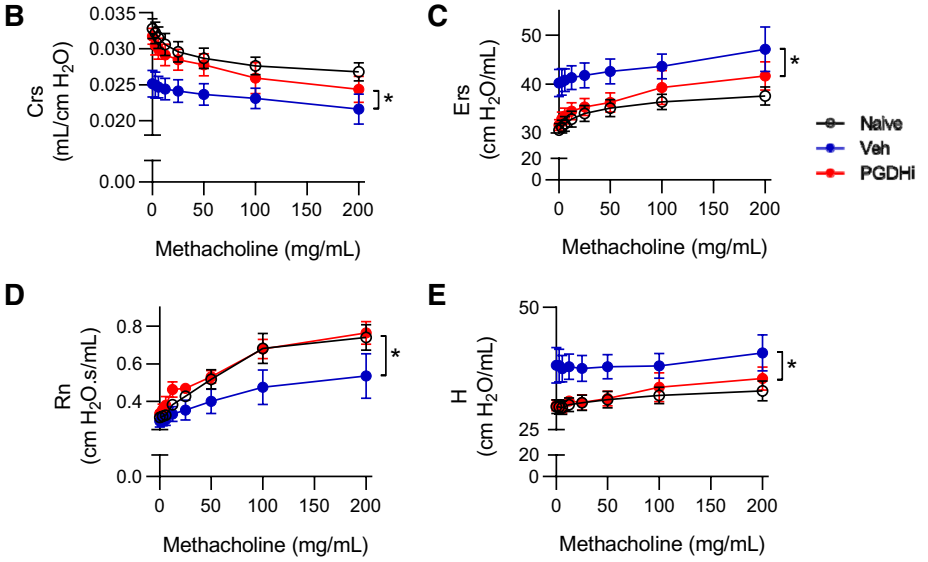

Figure 4. PGDHi mitigates the loss of pulmonary compliance and airway resistance observed in bleomycin-treated mice. PGDHi and vehicle treatment was administered through day 50 post-bleomycin administration. (**A**) Table depicting mean percentage of initial body weight, maximum baseline static lung compliance (mL per cm H_2O), mean inspiratory capacity (mL), and mean number of cells collected in bronchoalveolar lavage fluid (BALF), in healthy naïve control mice and Vehicle- and PGDHi-treated mice 50 days post-bleomycin administration. ± SEM. n = 3 mice/group. (**B**–**E**) Dynamic respiratory system compliance (Crs), respiratory system elastance (Ers), Newtonian airway resistance (Rn), and tissue elastance (H), measured using the forced oscillation technique at indicated doses of methacholine. Mean ± SEM depicted. n = 3 mice/group. $^*P < 0.05$.

choalveolar lavage fluid, as compared to vehicle-treated counterparts (Fig. 4A). Additionally, upon methacholine challenge, PGDHi-treatment resulted in significantly increased forced oscillation technique measurements of dynamic respiratory system compliance (Crs) and decreased respiratory system elastance (Ers; Fig. 4B,C). The bleomycin-induced loss in airway responsiveness to methacholine as Newtonian airway resistance (Rn), a measure of airflow in central airways, was also significantly reversed by PGDHi such that responses did not differ from naïve mice (Fig. 4D). Lastly, the rigidity of peripheral alveoli and lung parenchyma, measured as tissue elastance (H), was significantly reduced with PGDHi as compared to vehicle treatment (Fig. 4E).

Endothelial cells, mast cells, and macrophages are PGDHi targets. Known cellular drivers of PF pathogenesis include alveolar epithelial cells and fibroblasts[1]. To identify the cell types that PGDHi may act directly on during PF, we dissociated lung tissue from healthy mice and isolated cell populations based on surface marker expression. General hematopoietic and stromal separation on the basis of CD45 demonstrated enzyme activity in both CD45 positive and negative cells (data not shown). Stromal 15-PGDH activity likely comprises endothelial cells as the CD31+ population demonstrated moderate activity enrichment, consistent with a recent report[32]. To further delineate the identity of the 15-PGDH+ hematopoietic cells, we fractionated on the basis of CD117 to enrich mast cells, which participate in pulmonary wound healing[33], and F4/80 to enrich alveolar macrophages, which are implicated in IPF pathogenesis[1] and have also recently been shown to express 15-PGDH[32]. Both $CD117^+$ and $F4/80^+$ preparations showed striking enzyme activity enrichment relative to negative counterpart cell fractions (Fig. 5A). Additionally, 15-PGDH staining colocalized with CD31, Toluidine blue, and F4/80 staining in serial sections (Fig. 5B). These data, together with the work of Bärnthaler et al.[32], identify alveolar macrophages, mast cells, and to a lesser extent, endothelial cells, as the likely targets of PGDHi therapy in murine PF.

PGDH+ cells are present in human lung. Taken together, our in vivo results strongly identify 15-PGDH as a therapeutic target in murine bleomycin-induced PF. To determine if therapeutic targets exist in human lung tissue, we characterized 15-PGDH expression in human lung sections incidentally removed on autopsy. 15-PGDH was expressed in 6 of 6 lung specimens examined, and localized to cells lining the alveoli and blood

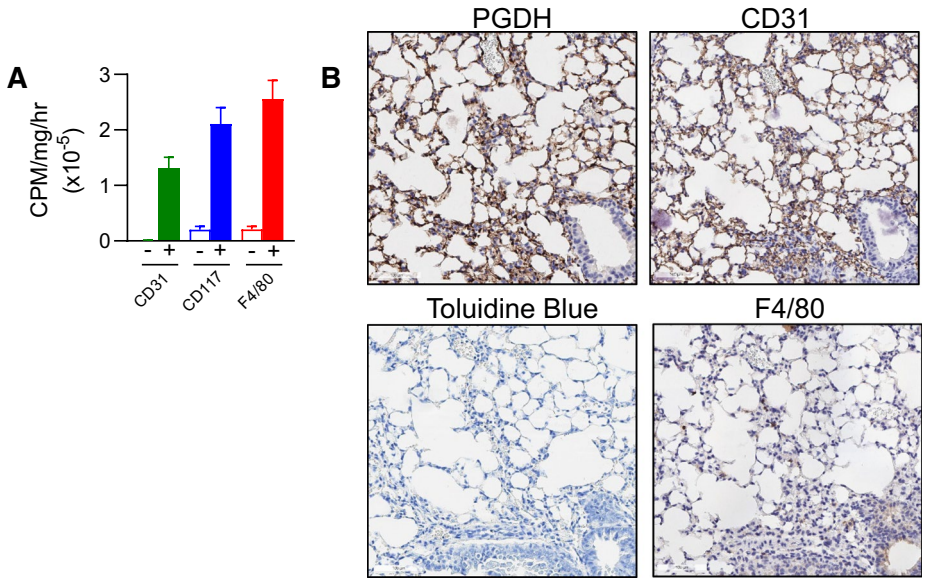

Figure 5. 15-PGDH is enriched in murine endothelial, mast, and macrophage cells. (**A**) Quantification of 15-PGDH enzymatic activity in the indicated cellular populations (filled bars represent the positive fraction and open bars represent the negative fraction for each surface marker) isolated from the lungs of healthy mice, measured over one hour and normalized to input total protein (in mg). Mean ± SEM is depicted. n = 4–6 mice per group. (**B**) Representative images of 15-PGDH, CD31, Toluidine Blue, and F4/80 staining (all in brown) in serial sections of healthy murine lung (20X). Scale bar represents 100 μm.

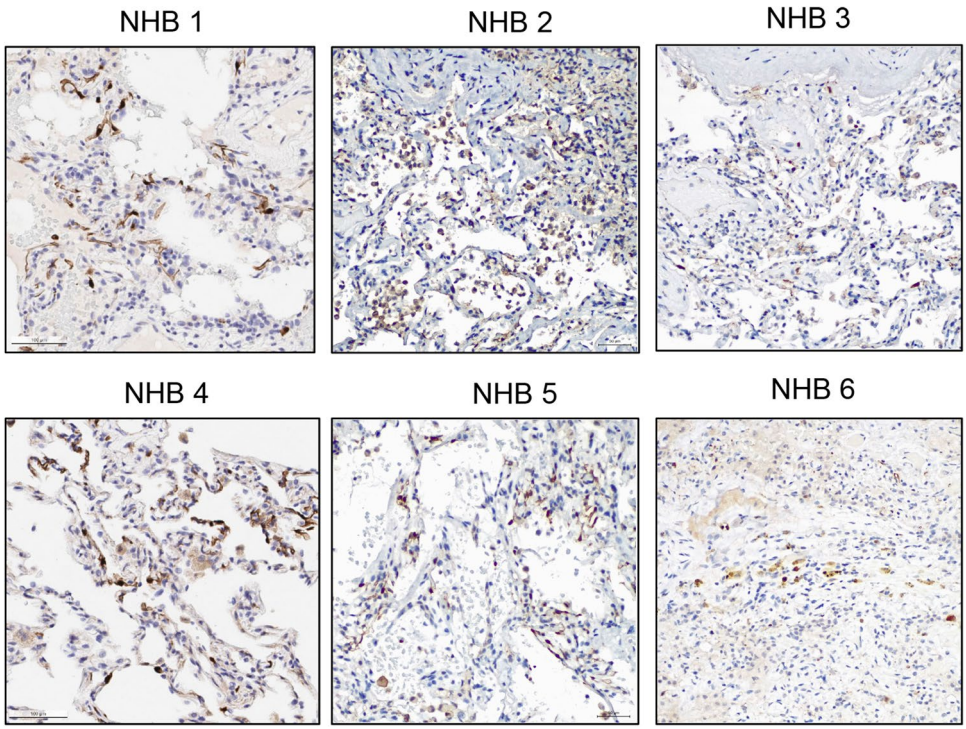

Figure 6. 15-PGDH is expressed in human lung. Representative images of 15-PGDH staining (brown) in normal human lung biopsies (NHB; 20X) from 6 unique donors. Scale bar represents 100 μm.

vessels (Fig. 6), consistent with previous reports[32,34]. The existence of PGDH+ cells in human lung tissue supports the notion that 15-PGDH inhibition may be a novel and effective therapy for IPF patients.

Discussion

In this study, we identified the presence of abundant 15-PGDH+ cells in murine pulmonary tissue. Compared to bone marrow and colon; tissues in which we have previously demonstrated enhanced regeneration and wound healing via pharmacologic 15-PGDH inhibition, lung tissue shows greater expression and enzyme activity. As PGE2 is well known to antagonize TGFβ-mediated fibrotic signaling, we tested the capacity for 15-PGDH inhibition to protect against PF pathology in mice exposed to bleomycin. Our data show that PGDHi strikingly attenuates early inflammation at day 7, which correlated with reduced weight loss and mortality. We find that continuous PGDHi treatment reduces the occurrence of fibrotic lesions and interstitial remodeling in the lung at day 35. Moreover, PGDHi attenuated lung dysfunction, as measured by changes in compliance, resistance, and tissue rigidity. Our data identify pulmonary endothelial cells, macrophages, and mast cells as the direct cellular targets of PGDHi, thus confirming and extending findings published in a recent report[32]. Lastly, the presence of PGDH+ cells in human pulmonary tissue identifies 15-PGDH as a potential novel therapeutic target in human IPF.

These data extend previous work demonstrating the capacity for PGE2 or specific agonism of EP2/EP4 receptors to attenuate TGFβ-mediated pro-fibrotic signaling in pulmonary fibroblasts[19,23–25], and provide a well-tolerated and efficacious alternative to the delivery of long-acting prostaglandin analogs[18]. Our dual effect on both acute inflammation and chronic fibrosis, as well as our finding that pulmonary endothelial cells, mast cells, and macrophages are highly 15-PGDH active, suggest multiple discrete mechanisms contribute to PGDHi-mediated protection. These results also indicate that systemic 15-PGDH inhibition may exert a more potent protective effect than targeted PGE2 delivery to endothelial cells[21] or alveolar macrophages[22] during IPF. Early in disease, PGDHi may improve alveolar epithelial wound repair, in a manner similar to that which has been demonstrated in the colonic epithelium[26]. Indeed, the concept that PGDHi may protect in part by improving alveolar stem and progenitor cell function is consistent with recent reports that senescent epithelial cells and fibroblasts drive IPF pathology[35]. Later in disease, and of particular clinical relevance, PGDHi reduces ECM protein expression and fibrotic remodeling in the lung, consistent with the impact of PGE2 administration or specific EP2/EP4 agonism, on human pulmonary fibroblasts from IPF patients[19]. Notably, PGDHi was associated with fewer fibrotic foci, preservation of alveolar architecture, and striking improvements to the dynamic compliance, resistance, and parenchymal rigidity of lungs upon forced oscillation analysis.

During the preparation of this manuscript, corroborating data was published by Bärnthaler et al.[32]. Both studies agree in the ability of PGDHi to increase local PGE2 levels, to prevent the accumulation of collagen, and to improve lung function in murine PF. Our work additionally demonstrates robust PGDH enzymatic activity in pulmonary tissue as compared to additional organs in which PGDHi has therapeutic efficacy[26]. Moreover, we demonstrate PGDHi-mediated amelioration of acute inflammatory pathology, including local diminution of *Il1b* and *Il6*, and systemic reductions in CXCL1, and TNFα, which likely contribute to the subsequent reductions in fibrosis and improvements in pulmonary function. These results are consistent with the known anti-inflammatory actions of PGE2[36]. Importantly, Bärnthaler et al. demonstrate that PGDHi initiated during fibrotic stage disease still confers protection[32]. Future studies to test the durability of the therapeutic effect after discontinuing PGDHi treatment are warranted.

PGDHi provides a novel and well-tolerated therapeutic approach to IPF, which is increasing in prevalence worldwide, particularly among aging populations. In the United States prevalence is estimated at 4.0 per 100,000 persons aged 18–34, and 227.2 per 100,000 persons among those > 75 years[37]. A history of cigarette smoking is the strongest risk factor, with additional risks including exposure to stone, wood, and organic dusts, and gastroesophageal reflux, which may contribute to lung injury via microaspiration[38,39]. While recent work has yielded greater insight into the pathogenesis of IPF and related progressive fibrosis that occurs in interstitial pneumonias of unknown cause, treatment options remain only partially effective. FDA approved therapies include Nintedanib, an inhibitor of nonreceptor and receptor tyrosine kinases, and Pirfenidone a small molecule of unknown mechanism. Neither are curative but demonstrate an ability to slow disease progression and can be combined with palliative care approaches to improve quality of life[38,39]. Patients deemed critical may be eligible for lung transplantation, which provides a 40–50% 5-year survival rate[40]. With a clear need for improved therapies for IPF and other interstitial lung diseases, our work demonstrates PGDHi holds significant promise either as a standalone therapy to prevent myofibroblast differentiation and reduce collagen deposition, or as a combination strategy with the currently approved therapies and palliative care.

Of interest, this work has additional therapeutic implications for disease states also characterized by fibrotic lesions. Primary myelofibrosis (PMF) is a rare bone marrow disorder characterized by abnormal blood cell production, extensive bone marrow scarring, activation of extramedullary hematopoiesis to the spleen, and a high incidence of leukemic transformation[41]. Median overall survival is only six years using current standards of care ruxolitinib, hydroxyurea, or bone marrow transplantation[42–44]. PGDHi may hold significant promise for PMF therapy, as inhibition of the TGFβ signaling axis has demonstrated efficacy in preclinical PMF models[45,46]. TGFβ transformation of fibroblasts plays a significant role in additional fibrotic diseases including hepatic, skin, and post-radiation induced fibrosis of multiple organs[47], as well. We propose that PGDHi-mediated disruption of myofibroblast differentiation will have therapeutic benefit in a number of these models and provide novel treatment strategies for these poor prognosis conditions.

Methods

Reagents. Bleomycin sulfate was purchased from Cayman Chemical and was dissolved in 0.9% sodium chloride to a concentration of 16 mg/mL. 80 mg bleomycin per kg mouse body weight was administered as a single dose at day 0 by retro-orbital injection under isoflurane anesthesia. For intratracheal instillation, 2 mg bleomycin per kg mouse body weight was administered to anesthetized, intubated mice by slowly instilling into

the trachea. (+)SW033291 was prepared in a vehicle of 10% ethanol, 5% Cremophor EL, 85% dextrose-5 water, at a concentration of 125 µg/200 µl for use at 5 mg/kg for a 25 g mouse. (+)SW033291 was administered by intraperitoneal injection, twice per day spaced by 8 h, beginning immediately after bleomycin administration and continuing through the duration of the experiment.

Animals. The animals described in this study were housed in the AAALAC accredited facilities of the CWRU School of Medicine. Standard Operating Procedures and reference materials are available from the IACUC Office for animal use. The animal health program was directed by the Case Animal Resource Center Director, W. John Durfee, DVM, Diplomate ACLAM, and provided by two full-time clinical veterinarians. Steady-state analysis and bleomycin administration was performed on female C57BL/6J mice obtained from Jackson Laboratories at 8 weeks of age. All animals were observed daily for signs of illness, and following bleomycin administration, mice were also weighed 2–3 times per week. Mice were housed in standard microisolator cages and maintained on a defined, irradiated diet and autoclaved water. Medical records and documentation of experimental use were maintained individually or by cage group. Veterinary technicians under the direction of the attending veterinarian provided routine veterinary medical care, if needed. Animal care and use was additionally monitored for training and compliance issues by the Director, Research Compliance IACUC. The Case Assurance number is A-3145-01, valid until April 30, 2023. All husbandry and experimental procedures were approved by the Case Western Reserve University Institutional Animal Care and Use Committee (IACUC) and we confirm that all procedures were performed in accordance with approved IACUC protocol 2013-0182.

Histological and immunohistochemical analysis. Animals were harvested via CO_2 inhalation followed by cervical dislocation and whole lungs excised and placed in 10% neutral buffered formalin for 24 h. Samples were transferred to PBS and shipped to Histowiz where they were embedded in paraffin, and sectioned at 4 µm. Immunohistochemistry was performed according to Histowiz protocols (https://home.histowiz.com/faq/). Histowiz defines their standard methods as the use of a Bond Rx autostainer (Leica Biosystems) with enzyme treatment using standard protocols, and detection via Bond Polymer Refine Detection (Leica Biosystems) according to manufacturer's protocol. Whole slide scanning (40×) was performed on an Aperio AT2 (Leica Biosystems).

Semiquantitative morphological evaluation. The degree of pulmonary inflammation and fibrosis in day 35 lung samples was semiquantitatively evaluated on Masson's Trichrome-stained sections of the whole lung, *in toto*. Briefly, we employed a previously reported semiquantitative morphological scoring system[28], in which 0: Normal lung; (1) Minimal areas of inflammation, epithelial hyperplasia and fibrosis, usually limited to subpleural foci in 1–3 lobes; (2) More frequent lesions; (3) All lobes exhibit lung lesions, which are not limited to subpleural foci; (4) Extensive lesions in at least 3 lobes; (5) Majority of all lobes affected by inflammation and fibrosis.

Real time PCR. On Day 0 and 7 post bleomycin induction, animals were harvested via CO2 inhalation followed by cervical dislocation and whole lungs excised and homogenized in RLT buffer. For comparison of bone marrow, colon, and lung, hindlimb marrow was flushed and the distal colon was dissected, prior to homogenization in RLT buffer. RNA isolation was performed using the RNAEasy Kit (Qiagen) and real-time PCR performed using commercial primers purchased from Applied Biosystems: IL2 (Mm00434256_m1), IL1B(Mm00434228_m1), IL6 (Mm00446190_m1), TNF (Mm00443258_m1), CXCL13 (Mm04214185_s1). Values were tabulated graphically with error bars corresponding to standard error of the means and compared using 2-tailed t-tests.

Multiplex ELISA. Peripheral blood from mice 7 days post-bleomycin exposure was collected into Microtainer serum-separator tubes (Becton–Dickinson) by submandibular cheek puncture. Whole blood was allowed to clot at room temperature and then spun at 6,000×*g* for 3 min to separate serum. Serum was removed and stored at -80 prior to analyzing with the V-PLEX ProInflammatory Panel 1 Mouse Kit (Meso Scale Diagnostics).

Lung mechanics. Mice were weighed and anesthetized with an intraperitoneal injection of ketamine/xylazine and placed in a supine position. Once mice were nonresponsive to toe pinch, midline tracheostomy was performed to insert a blunt tip cannula. Mice were then paralyzed with pancuronium bromide and mechanically ventilated by the flexiVent system (SCIREQ, FX2 module) with continuous ECG monitoring. The maximum baseline static compliance was measured using computer software slope-fit of a quasi-static pressure–volume loop (Salazar–Knowles equation). Dynamic compliance (Crs), elastance (Ers), Newtonian airway resistance (Rn), and tissue elastance (H) were calculated by forced oscillation technique (Snapshot-150 and Quick Prime-3). Following two recruitment breaths (30 cm H_2O for 3 s), increasing doses of methacholine (0–200 mg/mL; Sigma-Aldrich) were administered over 10 s via an in-line ultrasonic nebulizer (AeroNeb, SCIREQ). After each methacholine dose, 6 dynamic measurements were made and the mean values were analyzed. Subsequently, the bronchoalveolar lavage fluid was collected by instilling 0.5 mL of PBS into the lung with a 10 s dwell time.

Cell separation. Briefly, lungs were minced and enzymatically-digested using previously described methods[48] to generate a single cell suspension. Cells were then isolated by surface marker expression using Miltenyi microbead kits and LS column separation. 15-PGDH enzymatic activity was measured in lysed cell fractions, or in homogenized whole organs, as previously reported[26]. Activity was then normalized to input pro-

tein and were tabulated graphically with error bars corresponding to standard error of the means and compared using 2-tailed t-tests.

Measurement of hydroxyproline content in lung lysate. Hydroxyproline was measured using the Hydroxyproline Assay Kit (Sigma-Aldrich), according to manufacturer's instructions.

Statistical analysis. Analysis was performed using GraphPad Prism software. Unpaired two-tailed Student's t-tests were used when two groups were compared. Statistical analyses performed for other datasets are described in the relevant figure legends. For body weight loss, data was analyzed using ordinary two-way ANOVAs with post-hoc Sidak's multiple comparisons tests. For overall survival time, Log-Rank (Mantel–Cox) tests were used to compare vehicle- versus PGDHi-treated mice. For lung mechanics, area under the curve was calculated and unpaired two-tailed Student's t-tests were used to compare vehicle versus PGDHi responses.

Received: 12 December 2019; Accepted: 23 June 2020
Published online: 15 July 2020

References

1. Lederer, D. J. & Martinez, F. J. Idiopathic pulmonary fibrosis. *N. Engl. J. Med.* **378**, 1811–1823. https://doi.org/10.1056/NEJMra1705751 (2018).
2. King, T. E. Jr., Pardo, A. & Selman, M. Idiopathic pulmonary fibrosis. *Lancet* **378**, 1949–1961. https://doi.org/10.1016/S0140-6736(11)60052-4 (2011).
3. Ashcroft, G. S., Horan, M. A. & Ferguson, M. W. Aging alters the inflammatory and endothelial cell adhesion molecule profiles during human cutaneous wound healing. *Lab. Invest.* **78**, 47–58 (1998).
4. Hecker, L. *et al.* Reversal of persistent fibrosis in aging by targeting Nox4–Nrf2 redox imbalance. *Sci. Transl. Med.* **6**, 231–247. https://doi.org/10.1126/scitranslmed.3008182 (2014).
5. Kolb, M., Bonella, F. & Wollin, L. Therapeutic targets in idiopathic pulmonary fibrosis. *Respir. Med.* **131**, 49–57. https://doi.org/10.1016/j.rmed.2017.07.062 (2017).
6. Wynn, T. A. Integrating mechanisms of pulmonary fibrosis. *J. Exp. Med.* **208**, 1339–1350. https://doi.org/10.1084/jem.20110551 (2011).
7. Ashitani, J. *et al.* Granulocyte-colony stimulating factor levels in bronchoalveolar lavage fluid from patients with idiopathic pulmonary fibrosis. *Thorax* **54**, 1015–1020. https://doi.org/10.1136/thx.54.11.1015 (1999).
8. Car, B. D. *et al.* Elevated IL-8 and MCP-1 in the bronchoalveolar lavage fluid of patients with idiopathic pulmonary fibrosis and pulmonary sarcoidosis. *Am. J. Respir. Crit. Care Med.* **149**, 655–659. https://doi.org/10.1164/ajrccm.149.3.8118632 (1994).
9. Guiot, J., Henket, M., Corhay, J. L., Moermans, C. & Louis, R. Sputum biomarkers in IPF: Evidence for raised gene expression and protein level of IGFBP-2, IL-8 and MMP-7. *PLoS ONE* **12**, e0171344. https://doi.org/10.1371/journal.pone.0171344 (2017).
10. Gregory, A. D. *et al.* Neutrophil elastase promotes myofibroblast differentiation in lung fibrosis. *J. Leukoc. Biol.* **98**, 143–152. https://doi.org/10.1189/jlb.3HI1014-493R (2015).
11. Takemasa, A., Ishii, Y. & Fukuda, T. A neutrophil elastase inhibitor prevents bleomycin-induced pulmonary fibrosis in mice. *Eur. Respir. J.* **40**, 1475–1482. https://doi.org/10.1183/09031936.00127011 (2012).
12. Misharin, A. V. *et al.* Monocyte-derived alveolar macrophages drive lung fibrosis and persist in the lung over the life span. *J. Exp. Med.* **214**, 2387–2404. https://doi.org/10.1084/jem.20162152 (2017).
13. Mills, C. D. M1 and M2 Macrophages: Oracles of health and disease. *Crit. Rev. Immunol.* **32**, 463–488 (2012).
14. Heukels, P., Moor, C. C., von der Thusen, J. H., Wijsenbeek, M. S. & Kool, M. Inflammation and immunity in IPF pathogenesis and treatment. *Respir. Med.* **147**, 79–91. https://doi.org/10.1016/j.rmed.2018.12.015 (2019).
15. Aschner, Y. & Downey, G. P. Transforming growth factor-beta: Master regulator of the respiratory system in health and disease. *Am. J. Respir. Cell Mol. Biol.* **54**, 647–655. https://doi.org/10.1165/rcmb.2015-0391TR (2016).
16. Mukherjee, S., Kolb, M. R., Duan, F. & Janssen, L. J. Transforming growth factor-beta evokes Ca^{2+} waves and enhances gene expression in human pulmonary fibroblasts. *Am. J. Respir. Cell Mol. Biol.* **46**, 757–764. https://doi.org/10.1165/rcmb.2011-0223OC (2012).
17. Lacy, S. H. *et al.* Human lung fibroblasts produce proresolving peroxisome proliferator-activated receptor-gamma ligands in a cyclooxygenase-2-dependent manner. *Am. J. Physiol. Lung Cell Mol. Physiol.* **311**, L855–L867. https://doi.org/10.1152/ajplung.00272.2016 (2016).
18. Failla, M. *et al.* 16,16-Dimethyl prostaglandin E2 efficacy on prevention and protection from bleomycin-induced lung injury and fibrosis. *Am. J. Respir. Cell Mol. Biol.* **41**, 50–58. https://doi.org/10.1165/rcmb.2007-0438OC (2009).
19. Mukherjee, S. *et al.* Prostaglandin E2 inhibits profibrotic function of human pulmonary fibroblasts by disrupting Ca(2+) signaling. *Am. J. Physiol. Lung Cell Mol. Physiol.* **316**, L810–L821. https://doi.org/10.1152/ajplung.00403.2018 (2019).
20. Moore, B. B. *et al.* Bleomycin-induced E prostanoid receptor changes alter fibroblast responses to prostaglandin E2. *J. Immunol.* **174**, 5644–5649. https://doi.org/10.4049/jimmunol.174.9.5644 (2005).
21. Marchetti, G. M. *et al.* Targeted drug delivery via caveolae-associated protein PV1 improves lung fibrosis. *Commun. Biol.* **2**, 92. https://doi.org/10.1038/s42003-019-0337-2 (2019).
22. Ivanova, V. *et al.* Inhalation treatment of pulmonary fibrosis by liposomal prostaglandin E2. *Eur. J. Pharm. Biopharm.* **84**, 335–344. https://doi.org/10.1016/j.ejpb.2012.11.023 (2013).
23. Garrison, G. *et al.* Reversal of myofibroblast differentiation by prostaglandin E(2). *Am. J. Respir. Cell Mol. Biol.* **48**, 550–558. https://doi.org/10.1165/rcmb.2012-0262OC (2013).
24. Kolodsick, J. E. *et al.* Prostaglandin E2 inhibits fibroblast to myofibroblast transition via E. prostanoid receptor 2 signaling and cyclic adenosine monophosphate elevation. *Am. J. Respir. Cell Mol. Biol.* **29**, 537–544. https://doi.org/10.1165/rcmb.2002-0243OC (2003).
25. Thomas, P. E., Peters-Golden, M., White, E. S., Thannickal, V. J. & Moore, B. B. PGE(2) inhibition of TGF-beta1-induced myofibroblast differentiation is Smad-independent but involves cell shape and adhesion-dependent signaling. *Am. J. Physiol. Lung Cell Mol. Physiol.* **293**, L417-428. https://doi.org/10.1152/ajplung.00489.2006 (2007).
26. Zhang, Y. *et al.* Tissue regeneration. Inhibition of the prostaglandin-degrading enzyme 15-PGDH potentiates tissue regeneration. *Science* **348**, aaa2340. https://doi.org/10.1126/science.aaa2340 (2015).
27. Desai, A. *et al.* A second-generation 15-PGDH inhibitor promotes bone marrow transplant recovery independently of age, transplant dose and granulocyte colony-stimulating factor support. *Haematologica* **103**, 1054–1064. https://doi.org/10.3324/haematol.2017.178376 (2018).

28. Izbicki, G., Segel, M. J., Christensen, T. G., Conner, M. W. & Breuer, R. Time course of bleomycin-induced lung fibrosis. *Int. J. Exp. Pathol.* **83**, 111–119. https://doi.org/10.1046/j.1365-2613.2002.00220.x (2002).
29. Santana, A., Saxena, B., Noble, N. A., Gold, L. I. & Marshall, B. C. Increased expression of transforming growth factor beta isoforms (beta 1, beta 2, beta 3) in bleomycin-induced pulmonary fibrosis. *Am. J. Respir. Cell Mol. Biol.* **13**, 34–44. https://doi.org/10.1165/ajrcmb.13.1.7541221 (1995).
30. Warshamana, G. S., Corti, M. & Brody, A. R. TNF-alpha, PDGF, and TGF-beta(1) expression by primary mouse bronchiolar-alveolar epithelial and mesenchymal cells: tnf-alpha induces TGF-beta(1). *Exp. Mol. Pathol.* **71**, 13–33. https://doi.org/10.1006/exmp.2001.2376 (2001).
31. Sun, L. *et al.* New concepts of IL-10-induced lung fibrosis: fibrocyte recruitment and M2 activation in a CCL2/CCR2 axis. *Am. J. Physiol. Lung Cell Mol. Physiol.* **300**, L341-353. https://doi.org/10.1152/ajplung.00122.2010 (2011).
32. Barnthaler, T. *et al.* Inhibiting eicosanoid degradation exerts antifibrotic effects in a pulmonary fibrosis mouse model and human tissue. *J. Allergy Clin. Immunol.* https://doi.org/10.1016/j.jaci.2019.11.032 (2019).
33. Campillo-Navarro, M. *et al.* Mast cells in lung homeostasis: Beyond type I hypersensitivity. *Curr. Respir. Med. Rev.* **10**, 115–123. https://doi.org/10.2174/1573398X10666141024220151 (2014).
34. Yan, M. *et al.* 15-Hydroxyprostaglandin dehydrogenase, a COX-2 oncogene antagonist, is a TGF-beta-induced suppressor of human gastrointestinal cancers. *Proc. Natl. Acad. Sci. USA* **101**, 17468–17473. https://doi.org/10.1073/pnas.0406142101 (2004).
35. Schafer, M. J. *et al.* Cellular senescence mediates fibrotic pulmonary disease. *Nat. Commun.* **8**, 14532. https://doi.org/10.1038/ncomms14532 (2017).
36. Gill, S. K. *et al.* The anti-inflammatory effects of PGE2 on human lung macrophages are mediated by the EP4 receptor. *Br. J. Pharmacol.* **173**, 3099–3109. https://doi.org/10.1111/bph.13565 (2016).
37. Raghu, G., Weycker, D., Edelsberg, J., Bradford, W. Z. & Oster, G. Incidence and prevalence of idiopathic pulmonary fibrosis. *Am. J. Respir. Crit. Care Med.* **174**, 810–816. https://doi.org/10.1164/rccm.200602-163OC (2006).
38. Raghu, G. *et al.* An official ATS/ERS/JRS/ALAT statement: Idiopathic pulmonary fibrosis: Evidence-based guidelines for diagnosis and management. *Am. J. Respir. Crit. Care Med.* **183**, 788–824. https://doi.org/10.1164/rccm.2009-040GL (2011).
39. Lee, J. S. *et al.* Does chronic microaspiration cause idiopathic pulmonary fibrosis?. *Am. J. Med.* **123**, 304–311. https://doi.org/10.1016/j.amjmed.2009.07.033 (2010).
40. Mason, D. P. *et al.* Lung transplantation for idiopathic pulmonary fibrosis. *Ann. Thorac. Surg.* **84**, 1121–1128. https://doi.org/10.1016/j.athoracsur.2007.04.096 (2007).
41. Vallapureddy, R. R. *et al.* Leukemic transformation among 1306 patients with primary myelofibrosis: Risk factors and development of a predictive model. *Blood Cancer J.* **9**, 12. https://doi.org/10.1038/s41408-019-0175-y (2019).
42. Cervantes, F. *et al.* New prognostic scoring system for primary myelofibrosis based on a study of the International Working Group for myelofibrosis research and treatment. *Blood* **113**, 2895–2901. https://doi.org/10.1182/blood-2008-07-170449 (2009).
43. Harrison, C. *et al.* JAK inhibition with ruxolitinib versus best available therapy for myelofibrosis. *N. Engl. J. Med.* **366**, 787–798. https://doi.org/10.1056/NEJMoa1110556 (2012).
44. Lofvenberg, E. & Wahlin, A. Management of polycythaemia vera, essential thrombocythaemia and myelofibrosis with hydroxyurea. *Eur. J. Haematol.* **41**, 375–381. https://doi.org/10.1111/j.1600-0609.1988.tb00212.x (1988).
45. Agarwal, A. *et al.* Bone marrow fibrosis in primary myelofibrosis: Pathogenic mechanisms and the role of TGF-beta. *Stem Cell Investig.* **3**, 5. https://doi.org/10.3978/j.issn.2306-9759.2016.02.03 (2016).
46. Yue, L. *et al.* Efficacy of ALK5 inhibition in myelofibrosis. *JCI Insight* **2**, e90932. https://doi.org/10.1172/jci.insight.90932 (2017).
47. Meng, X. M., Nikolic-Paterson, D. J. & Lan, H. Y. TGF-beta: The master regulator of fibrosis. *Nat. Rev. Nephrol.* **12**, 325–338. https://doi.org/10.1038/nrneph.2016.48 (2016).
48. Wang, J., Niu, N., Xu, S. & Jin, Z. G. A simple protocol for isolating mouse lung endothelial cells. *Sci. Rep.* **9**, 1458. https://doi.org/10.1038/s41598-018-37130-4 (2019).

Author contributions

J.N.P.S. conceived the hypothesis, designed the experiments, collected and interpreted the data, and wrote the manuscript. M.D.W. collected and interpreted the data. A.P.J. and K.F.C. collected the data. T.M.R. collected and interpreted the lung mechanics data and revised the manuscript. S.D.M. conceived the hypothesis and revised the manuscript. A.B.D. conceived the hypothesis, designed the experiments, wrote the manuscript, and provided final approval of the manuscript. All authors have read the complete manuscript and provided final approval.

Competing interests

A.B.D. and S.D.M. hold patents relating to use of 15-PGDH inhibitors that have been licensed to Rodeo Therapeutics. S.D.M. is a founder of Rodeo Therapeutics, and S.D.M. and A.B.D. are consultants to Rodeo Therapeutics. Conflicts of interest are managed according to institutional guidelines and oversight by Case Western Reserve University. No conflict of interest pertains to any of the remaining authors.

Additional information

Supplementary information is available for this paper at https://doi.org/10.1038/s41598-020-68336-0.

Correspondence and requests for materials should be addressed to S.D.M. or A.B.D.

Reprints and permissions information is available at www.nature.com/reprints.

Publisher's note Springer Nature remains neutral with regard to jurisdictional claims in published maps and institutional affiliations.